Yuan, Han and Zhou, Peilin and Mei, Ning (2017) Numerical and experimental investigation on the ballast flushing system. Ocean Engineering, 130. pp. 188-198. ISSN 0029-8018 , http://dx.doi.org/10.1016/j.oceaneng.2016.12.003

This version is available at https://strathprints.strath.ac.uk/59578/

1 **Numerical and experimental investigation on the ballast flushing system**

2 **Han Yuan[1*], Peilin Zhou[2] and Ning Mei[1]**

3 *1. College of Engineering, Ocean University of China, 238 Songling Road, Laoshan*

4 *district, Qingdao 266100, China*

5 *2. Department of Naval Architecture and Marine Engineering, University of*

6 *Strathclyde, Glasgow G4 0LZ, United Kingdom*

7

8 Phone/Fax: +86-532-66781105,

9 E-mail: hanyuan@ouc.edu.cn

10 Address: 238 Songling Road, Laoshan district, Qingdao 266100, China

11

12 **Abstract**

13 The ballast sediments deposit not only provide the breeding ground for the survival

14 organisms, but also affect the weight balance of the ship and even accelerate the

15 corrosion of the ballast tank. In this work the performance of a ballast water flushing

16 system for the 138,000 m^3 LNGC (Liquefied Natural Gas Carrier) double bottom

17 cargo ship is studied. A simulation model of the ballast tank was made to conduct the

18 numerical analysis. Besides, a scaled experimental setup was established on basis of

19 the similarity principle. With different injecting velocities at the flushing inlet, the

20 sediments distribution in the ballast tank is investigated and the energy consumption

21 of the circulating pump is studied. The results show that by flushing the ballast water

22 on the bottom, the sediments first accumulate at the far end, with the sediments

23 volume fraction climbs up to 10-30%, before gradually getting removed over time.

24 Further, higher inlet velocity leads to a more rapid decrease of average sediments

25 proportion in the ballast tank over time, but the energy consumption in circulating

26 pump significantly increases as well. The required power for this proposed ballast

27 water flushing system is within the common range and thus applicable in the cargo

28 ship.

29 **Keywords:** Ballast water; sediments; flushing; CFD.

30

1. Introduction

32 Negative environmental impacts made by the uptake and discharge of ballast water

33 are great challenge for international shipping. The non-indigenous species (NIS)

34 transported in the ballast tank may cause harm to native ecosystems [1, 2] and these

35 invasive species can even contribute to animal extinctions in local area [3-5]. In

36 response to this challenge, the International Maritime Organization (IMO) instituted a

37 performance standard of "Regulation D-2" for ballast water treatment management

38 [6-8]. In this regulation, limitations on both the size and the quantity of the remained

39 organisms in the treated ballast water are made to exclude microbes and viable

40 microorganisms from discharged ballast water [9]. To meet the requirement of the

41 IMO convention, different sorts of ballast water management technologies including

42 oxidation by chlorine/ozone and the ultraviolet radiation (UV) method are proposed

43 by researchers.

44 Although dozens of shipboard treatment systems have been certified as meeting

45 ballast water discharge standards till now, their application in eliminating invasive

46 species is not that satisfactory[10, 11]. It should be noted that only the maximum

47 amount of living organisms is restricted according to Regulation D-2, nevertheless,

48   the remaining sediments in the ballast water is still not concerned. Studies in

49   references [12, 13] pointed out that the soil sediments mainly consist of the clay, silt

50   and sand, with the particle diameter from less than 2μm to 2mm. Moreover, these soil

51   sediments are admitted with ballast water during the ballasting. Although most of the

52   large-size organisms (>10μm) gets inactivated according to Regulation D-2, a tiny

53   fraction of organisms cannot be totally removed from the loaded ballast water, and

54   these soil sediments turn to be the perfect breeding ground for the survival organisms

55   [14-16].

56   In fact, providing the habitat for organisms is only part of negative impacts that the

57   ballast water sediments could induce. On one hand, it is found that The sediments at

58   the bottom of the ballast tanks in a double hull cargo vessel can accumulate up to 30

59   cm depth within only two years operation [17]. According to current Rules and

60   Regulations of respective Classification Societies, sediments in ballast water tank can

61   only be systematically removed during the mandatory dry docking, and the interval is

62   usually made in every five years [18]. With such a long period of time the sediments

63   tend to be compacted and the sediments removing work becomes a great challenge.

64   On the other hand, the ballast sediments also affect the weight balance of the ship.

65   Due to non-uniform distribution in the ballast tanks, the loading and unloading of

66   ballast have to be cautious, because the excessive stresses can potentially lead to a

67   ship breaking during incorrectly unloading [19].

68   Furthermore, the corrosion of the ballast tank is another negative impact induced by

69   the ballast sediments. The sulphate reducing bacteria (SRB) and acid producing

70   bacteria (APB) that living in the sediments can bring significant microbiologically

71   influenced corrosion (MIC) [20, 21]. Compared with the electrochemical oxidation

72   process, the corrosion speed of MIC is greatly accelerated and thus unpredictable.

73 This paper proposed a solution for this problem. With the flushing system, the

74 unfiltered sediments along with the regrown organisms can be removed when needed

75 In this paper, a ballast water flushing system is proposed. By circulating the ballast

76 water in the tank, the deposits of sediments can be suspended and removed before

77 getting compacted on the tank bottom. A simulation model of the ballast tank was

78 made; an experimental setup was established on basis of the similarity principle.

79 Further, with four different ejecting velocities, both numerical and experimental

80 studies were conducted to evaluate the performance of this flushing system.

81

82 2. System description

83 In this work the ballast water system of the 138,000 m^3 LNGC (Liquefied Natural Gas

84 Carrier) double bottom cargo ship [22] is investigated. The volume of cargo ballast

85 water system takes up to 56,090 m^3 in total. Figure 1 shows the structure of a single

86 block of ballast tank in the cargo ship. As is shown, lines of longitudinal are arranged

87 on the inner side of the ballast tank and drain holes are provided on the bottom

88 longitudinal. Besides, the ballast water pipes (inlet-pipe and outlet-pipe) are arranged

89 in the corner, on which a row of jet holes (inlets) are placed along the inflow-pipe

90 while a row of exit holes (outlets) are placed along the outflow-pipe. Besides, a

91 hydrocyclone [23] is introduced between the outflow-pipe and the circulating pump to

92 separate the sediments from the ballast water. The size of a single block of ballast

93 tank is $6700 \times 3000 \times 2000 (mm)$, and the size of inlets/outlets on the ballast water

94 pipes is $100 \times 10 (mm)$.

95　　With the assistance of the circulating pump, the ballast water is first pumped into the

96　　inflow-pipe and then ejected through the inlets, and in this way the deposits of

97　　sediments are stirred up. Further, the suspended sediments, along with the ballast

98　　water, get sucked into the outflow-pipe through the outlets. Then the mixture of water

99　　and sediments is separated in the hydrocyclone before pumped back into the ballast

100　　tank. As ballast water flows into the hydrocyclone, a cyclonic flow is produced and

101　　the centrifugal force drives the sediments toward the outer wall, so the clean water

102　　can flow through the centre of the hydrocyclone into the circulating pump. Thus the

103　　ballast water circulates around the ballast tank and the bottom sediments deposits are

104　　suspended and then removed from the ballast water.
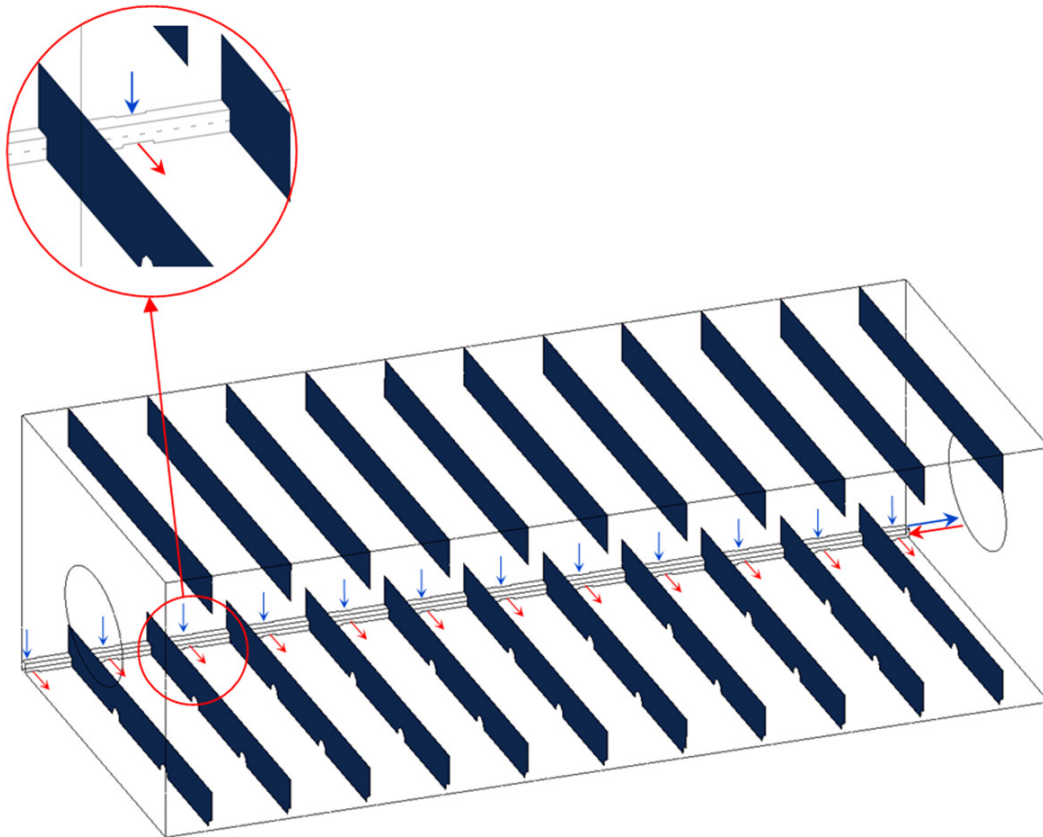
105
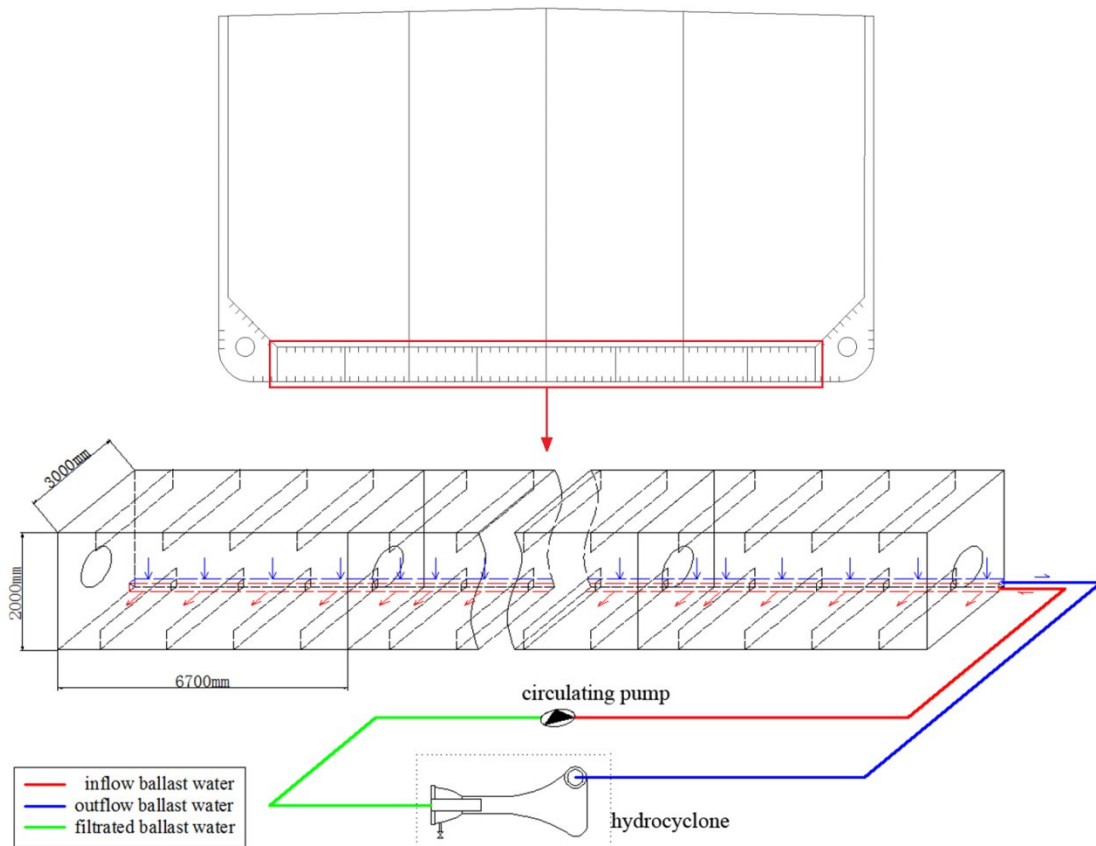
107　　　　　　　　　Figure 1 Schematic of ballast water flushing system

108   **3.   Simulation setup**

109   The numerical model for the ballast tank consists of a row of inlets along the inflow-

110   pipe, a row of outlets along the outflow-pipe and longitudinal with drain holes on the

111   inner side of the tank, as shown in Figure 2.

112

113   Figure 2 Ballast tank model for simulation

114

115   **3.1.   Modelling equations**

116   The mixture model, a kind of Eular-Eular multiphase model, is used in this simulation.

117   The two phases of water and sediment are treated as interpenetrating continua in the

118   mixture model. Besides, the momentum and continuity equations of the mixture and

119   the volume fraction equations of the secondary phase are solved. Compared with a

120 full Eulerian multiphase model, the mixture model is simpler, and more suitable for

121 the cases that the interphase laws are unknow. Simultaneously, the RNG $k-\varepsilon$ model

122 is selected as the turbulence model for the simulation. The RNG (Renormalization

123 Group) $k-\varepsilon$ model is a refined Standard $k-\varepsilon$ model, which is also derived from the

124 instantaneous Navier-Stoke equations and follows the $k-\varepsilon$ (turbulent kinetic energy

125 and dissipation rate) two equations turbulence modelling framework. But compared

126 with the Standard $k-\varepsilon$ model, the RNG $k-\varepsilon$ model introduces more terms of

127 dissipation in transport equation, which make it more accurate for rapidly strained

128 flows and swirling flows. Besides, this model accounts for low-Reynolds-number

129 effects and provides not constant values but an analytical formula for turbulent

130 Prandtl numbers. All of these refinements make the RNG $k-\varepsilon$ model more

131 appropriate for current simulation.

132

133 Governing equations:

134 The continuity equation is given as follow:

135 $$\frac{\partial}{\partial t}(\rho_m) + \frac{\partial}{\partial x_i}(\rho_m \vec{u}_m) = 0 \tag{1}$$

136 The momentum equation for the mixture is given as follow:

137 $$\frac{\partial}{\partial t}(\rho_m \vec{u}_m) + \frac{\partial}{\partial x_j}(\rho_m \vec{u}_m \vec{u}_m) = -\frac{\partial p}{\partial x_i} + \frac{\partial}{\partial x_j}[\mu_m(\frac{\partial}{\partial x_i}\vec{u}_m + \frac{\partial}{\partial x_j}\vec{u}_m)] + \rho_m \vec{g} - \frac{\partial}{\partial x_j}[\rho_m \overline{u_i' u_j'}] \tag{2}$$

138 Where $\vec{u}_m$ is the mass-averaged velocity, ρ_m is the mixture density, α_s and α_f are the

139 volume fraction of water phase and sediment phase, respectively, μ_m is the viscosity

140   of the mixture, $u_i^{'}$ is the turbulent velocity fluctuation. These terms can be written as

141   follows:

142    $$\overset{r}{u}_m = \frac{\sum_{k=1}^{n} \alpha_k \rho_k \overset{r}{u}_k}{\rho_m} = \frac{\alpha_s \rho_s \overset{r}{u}_s + \alpha_f \rho_f \overset{r}{u}_f}{\rho_m}$$ (3)

143    $$\rho_m = \alpha_s \rho_s + \alpha_f \rho_f$$ (4)

144    $$\mu_m = \alpha_s \mu_s + \alpha_f \mu_f$$ (5)

145    $$\alpha_s + \alpha_f = 1$$ (6)

146   Moreover, the Reynolds-stress tensor $-\rho_m \overline{u_i^{'} u_j^{'}}$ can be written as:

147    $$-\rho_m \overline{u_i^{'} u_j^{'}} = -\frac{2}{3} \rho_m k \delta_{ij} + \mu_t (\frac{\partial}{\partial x_i} \overset{r}{u}_m + \frac{\partial}{\partial x_j} \overset{r}{u}_m)$$ (7)

148    $$\mu_t = C_\mu \rho_m \frac{k^2}{\varepsilon}$$ (8)

149   Where k is the turbulent kinetic energy, ε is the turbulent dissipation rate, δ_{ij} is the

150   Kronecker delta. μ_t is the eddy viscosity, C_μ is a constant.

151   In addition, the momentum equation for the mixture is not closed unless the

152   Reynolds-stress tensor term is provided. This term can be obtained with assistance of

153   the turbulence model shown as follow.

154   The transport equations for the RNG $k-\varepsilon$ model can be described as follows:

155    $$\frac{\partial}{\partial t}(\rho k) + \frac{\partial}{\partial x_j}(\rho k \overset{r}{u}) = \frac{\partial}{\partial x_i}(\alpha_k \mu_{eff} \frac{\partial}{\partial x_i} k) + G_k + G_b - \rho\varepsilon$$ (9)

156 $$\frac{\partial}{\partial t}(\rho\varepsilon) + \frac{\partial}{\partial x_j}(\rho\varepsilon\overset{r}{u}) = \frac{\partial}{\partial x_i}(\alpha_\varepsilon\mu_{eff}\frac{\partial}{\partial x_i}\varepsilon) + C_{1\varepsilon}\frac{\varepsilon}{k}(G_k + C_{3\varepsilon}G_b) - C_{2\varepsilon}\rho\frac{\varepsilon^2}{k} - R_\varepsilon \qquad (10)$$

157 Where

158 $$\mu_{eff} = \mu + \mu_t \qquad (11)$$

159 $$G_k = \mu_t S^2 \qquad (12)$$

160 $$S = \sqrt{2S_{ij}S_{ij}} \qquad (13)$$

161 $$S_{ij} = \frac{1}{2}(\frac{\partial}{\partial x_i}\overset{r}{u}_m + \frac{\partial}{\partial x_j}\overset{r}{u}_m) \qquad (14)$$

162 In the $k-\varepsilon$ equations, G_k is the generation of turbulence kinetic energy due to the

163 mean velocity gradients, G_b is the generation of turbulence kinetic energy due to

164 buoyancy, which is neglected in this simulation, α_k and α_ε are the inverse effective

165 Prandtl numbers for k and ε, μ_{eff} is the effective viscosity, $C_{1\varepsilon}$, $C_{2\varepsilon}$ and $C_{3\varepsilon}$ are

166 turbulence model constants.

167 R_ε is the effects of rapid strain and streamline curvature, which reflects the main

168 difference between the RNG and standard $k-\varepsilon$ model. It can be written as:

169 $$R_\varepsilon = \frac{C_\mu\eta^3(1-\eta/\eta_0)}{1+\beta\eta^3}\frac{\varepsilon^2}{k} \qquad (15)$$

170 Where

171 $$\eta = \frac{k}{\varepsilon}S \qquad (16)$$

172 In the simulation, the values of above constants are taken as: $\alpha_k=\alpha_\varepsilon=1.39$, $\beta=0.012$,

173 $\eta_0=4.38$, $C_{1\varepsilon}=1.42$, $C_{2\varepsilon}=1.68$, $C_{3\varepsilon}=0$, $C_\mu=0.0845$.

3.2.   Simulation method validation

The sedimentation of sediments in the tank is a classic problem, which has been

extensively studied [24-28]. Therefore in this section, the reliability of above

mathematic model for sedimentation simulation is validated by selecting the

sedimentation tank in Ref. [24] as the research object. The geometry of the

sedimentation tank for the simulation is based on the experiment. The tank is a

rectangular one, with the length of 200 cm, width of 50cm and height of 31cm. The

inlet height is 10cm and the weir height is 30cm. The flow field and sediment

concentration of the sedimentation tank is simulated by utilizing the RNG $k-\varepsilon$-

mixture model in this paper. The boundary condition and initial condition in this

simulation is assigned the same as that in the experimental research in Ref. [24]. The

simulation results are compared with the experimental results, shown in Figure 3. It is

found that the numerical simulation results show a good match with the experimental

results. Both the flow field and the sediment concentration distribution of the

sedimentation tank are well predicted, which indicates that the turbulence model and

multiphase model utilized in this study is adaptable for the sedimentation simulation.

191   (a)

x=1.21m   x=1.58m   x=1.95m

192
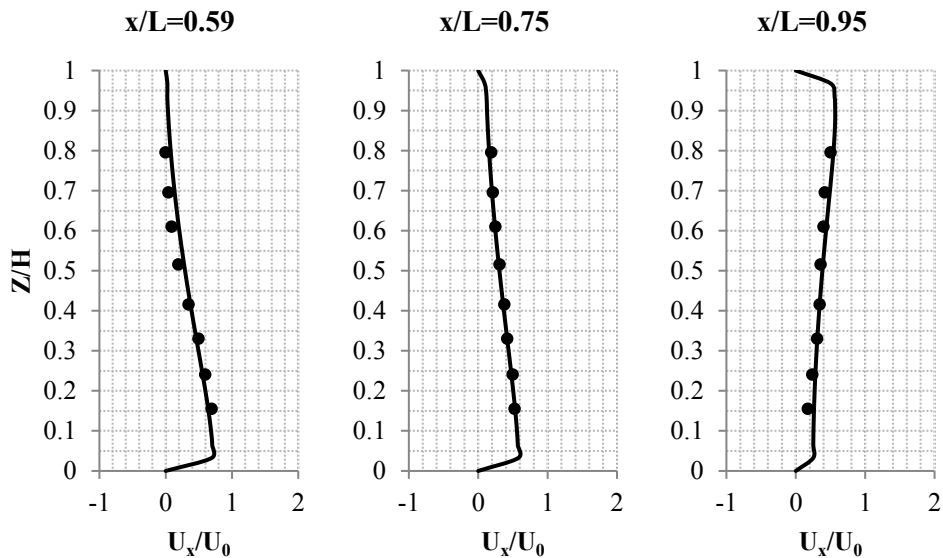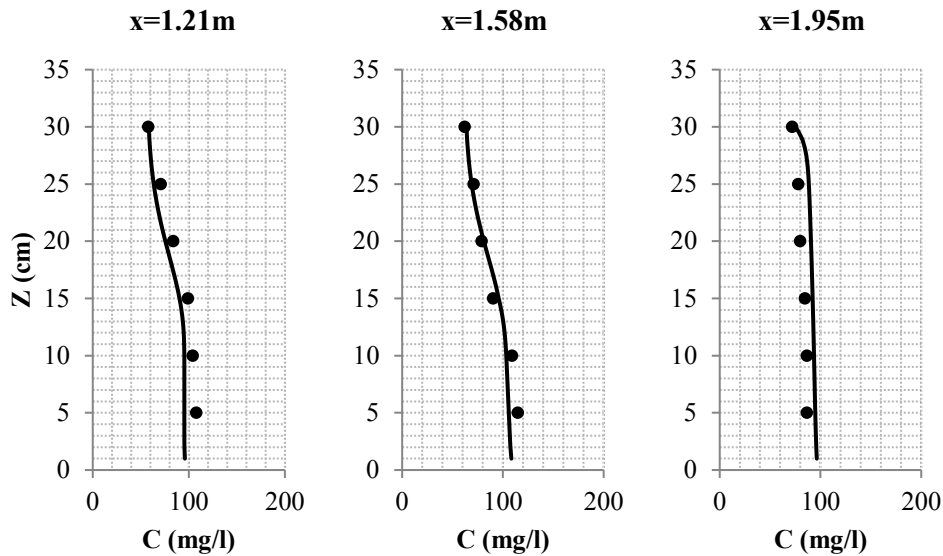
193   (b)

— Simulation result with proposed mathematic model
● Experimental result in Ref. [20]

194

Figure 3 Comparison of simulation and experimental results: (a) dimensionless x-

velocity of suspended sediments; (b) vertical distribution concentration of suspended

sediments at different locations

3.3. Initial conditions and boundary conditions

It is known that the thickness of accumulated sediment in the ballast tank varies from

a few millimetres to several centimetres, but in most tanks is less than 50mm [29, 30].

Meanwhile, according to A. Tamburini [31, 32], the initial sediments volume fraction

on the bottom is experimentally measured at approximately 60%, so in this simulation,

the thickness of accumulated sediments on the vessel bottom is assumed to be 20mm

and the initial sediments volume fraction is made at 60%. Moreover, based on the

experimental data, the measured bulk density of sediments is made at 1500 kg/m^3 and

the median particle diameter is 11.64μm. The density of seawater is 1025 kg/m^3.

Besides, the magnitude of the gravitational acceleration is 9.8 m/s^2. Further, in the

208 simulation, the velocity-inlet boundary condition is assigned for the inlets on the

209 inflow-pipe. The magnitude of the inlet velocities are assigned at 4 constant values (at

210 5m/s, 10m/s, 15m/s, 20m/s, respectively) and the velocity direction is normal to the

211 inlet face. Besides, the pressure-outlet boundary condition is applied for the outlets on

212 the outflow-pipe.

213 **3.4. Monitoring plane and lines for simulation model**

214 A monitoring plane is used to obtain the sediments distribution of the ballast water.

215 Since the sediments are flushed and suspended by the ejected water along the ballast

216 tank bottom from left corner to right corner, the right corner sediments would be the

217 latest removed. Thus, 5 monitoring lines locate in the bottom right corner are used to

218 evaluate the suspending condition of the ballast tank. The location of these 5

219 monitoring lines are assigned at z=0mm, 10mm, 20mm, 30mm and 40mm, among

220 which lines of z=0mm, 10mm and 20mm are located in the initial sediments layer and

221 lines of z=30mm and 40mm are located above the initial sediments layer. These

222 monitoring plane and lines are shown in Figure 4.
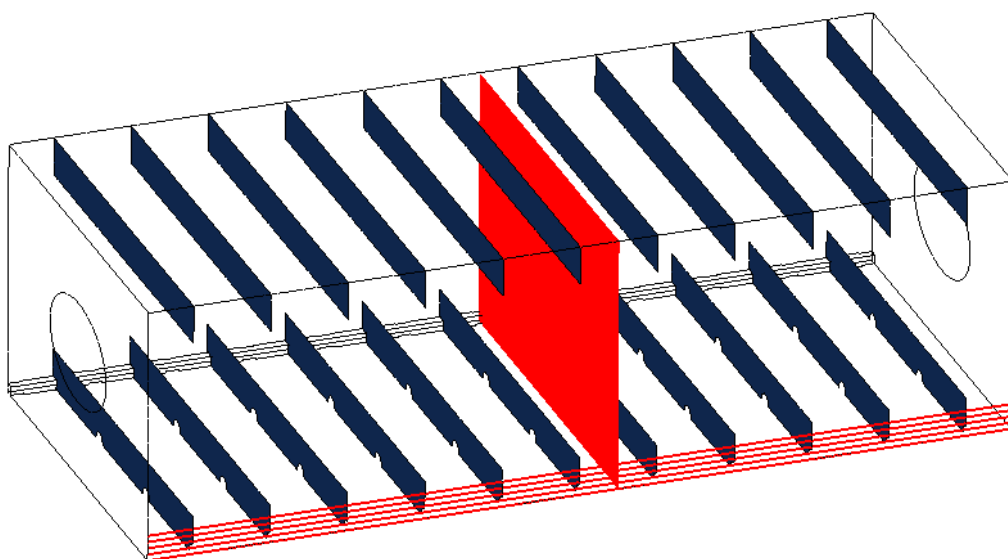
223

224 Figure 4 Monitoring plane and lines for simulation results analysis

225   **4.   Experimental setup**

226   **4.1.   Test bench description**

227   A 1:10 scaled model of an acrylic ballast tank unit along with the test system was

228   constructed, shown in Figure 5. The bottom sediment in the ballast tank is

229   continuously flushed by the seawater that pumped from the seawater tank. The

230   outflow ballast water is then collected in the sediments tanks. In the experiments, the

231   injecting velocity of seawater at the inlet is controlled by the volume flow rate that

232   monitored with a flow meter. Further, a camera is used to monitor the sediments

233   distribution in the ballast tank.
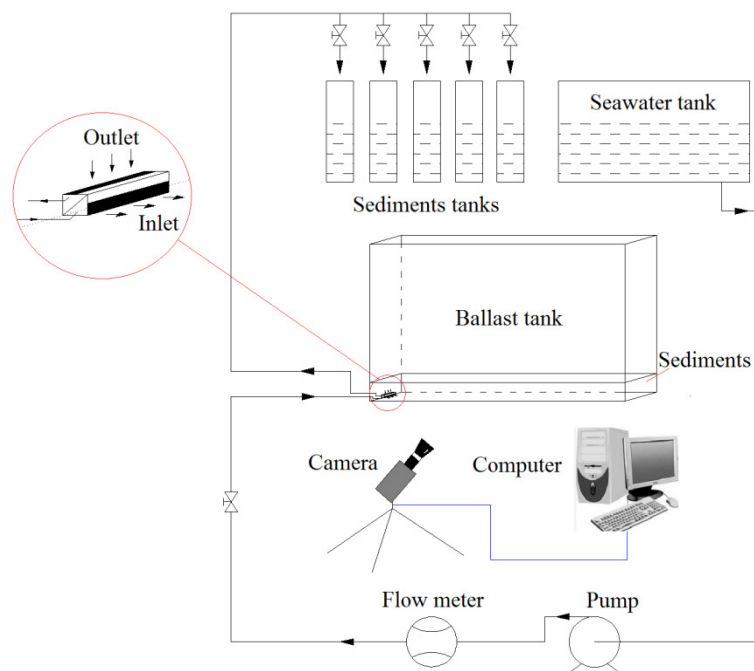
234

235   Figure 5 Experimental system

236   The real-time measurement of the sediments proportion that remains in the ballast

237   tank is difficult. A. Tamburini [33] provided a method of quantifying the sediments

238   proportion in the entire tank. By introducing an impeller and measuring the density

239   caused pressure variation, the percentage of suspended solids can be calculated.

240 However, the impact of stirring process on the pressure of tank bottom is neglected in

241 this method, which leads to a low precision in the measurement.

242 In this study, the mean sediments proportion in the ballast tank is calculated based on

243 the weight of remained sediments in the ballast tank, which is ultimately measured by

244 the weight of sediments in the sediments tanks. The removed sediments are first

245 collected in the sediments tanks, and then weighted by oven drying method: after

246 being dried in the oven for 12 hours, the sediments are cooled to ambient temperature

247 in the dryer and weighted by an analytical balance. It is noted that a test consists of 3

248 replicates to arrive at the final result.

249 **Table 1 Parameters of instruments**

Analytical balance	0~0.2 kg, ±0.05%
Flowmeter	0.10~10 m^3/h, ±1.5%

250

251 **4.2. Experimental plan**

252 In order to obtain a similar sediment removing process, the Froude number, which

253 represents the ratio of the flow inertia to the external field, is selected as the key

254 dimensionless number in the experiments[19], and the experimental parameters of

255 both the injecting velocity at the inlets and the required sediments removing time are

256 fixed based on the similarity principle. The Froude number is defined as:

257 $$Fr = \frac{u}{\sqrt{gl}}$$ (17)

258 Where, u is the characteristic velocity of the flow, l is the characteristic length scale

259 of the flow.

260   Based on the similarity principle, the velocity scale and time scale for the

261   experimental model can be determined as follows:

262    $u_r = T_r = \sqrt{l_r}$ (18)

263   Where, l_r is the geometric scale of the experimental model, fixed at 1:10.

264   In the tests, the thickness of accumulated sediments on the tank bottom is 2mm and

265   the initial sediments volume fraction is made at 60%. The bulk density of sediments is

266   made at 1500 kg/m^3 and the measured median particle diameter is 11.64μm.

267   According to the calculation, the initial weight of the accumulated sediments on the

268   tank bottom is 328.86g. Before conducting the experiments, these sediments are first

269   fully suspended in the entire tank and then deposited in the tank, this process is to

270   make sure they are uniformly distributed after settling down on the bottom.

271   The experimental plan is listed in Table 2.

272   **Table 2 Experimental plan**

| Experimental conditions	Inlet velocity m/s	Flow rate in pump L/s
Test 1	1.58	0.0158
Test 2	3.16	0.0316
Test 3	4.74	0.0474
Test 4	6.32	0.0632

273

274   **5.   Results and discussions**

275   **5.1.   Sediments distribution on the tank bottom**

276   Considering that the sediments discharged from the outlet of outflow-pipe are

277   separated in the hydrocyclone (with a relatively high separation efficiency of 98%),

278　thus, once the average proportion of the sediments in the ballast tank is less than 2%,

279　the sediments in the ballast tank can be considered adequately removed. In the

280　simulation, 4 inlet velocities of 5m/s, 10m/s, 15m/s and 20m/s are assigned. The

281　isosurfaces of sediments proportion above 2% at 600s are obtained and shown in

282　Figure 6.

(a)　　　　　　　　　　　　　　　　(b)

(c)　　　　　　　　　　　　　　　　(d)
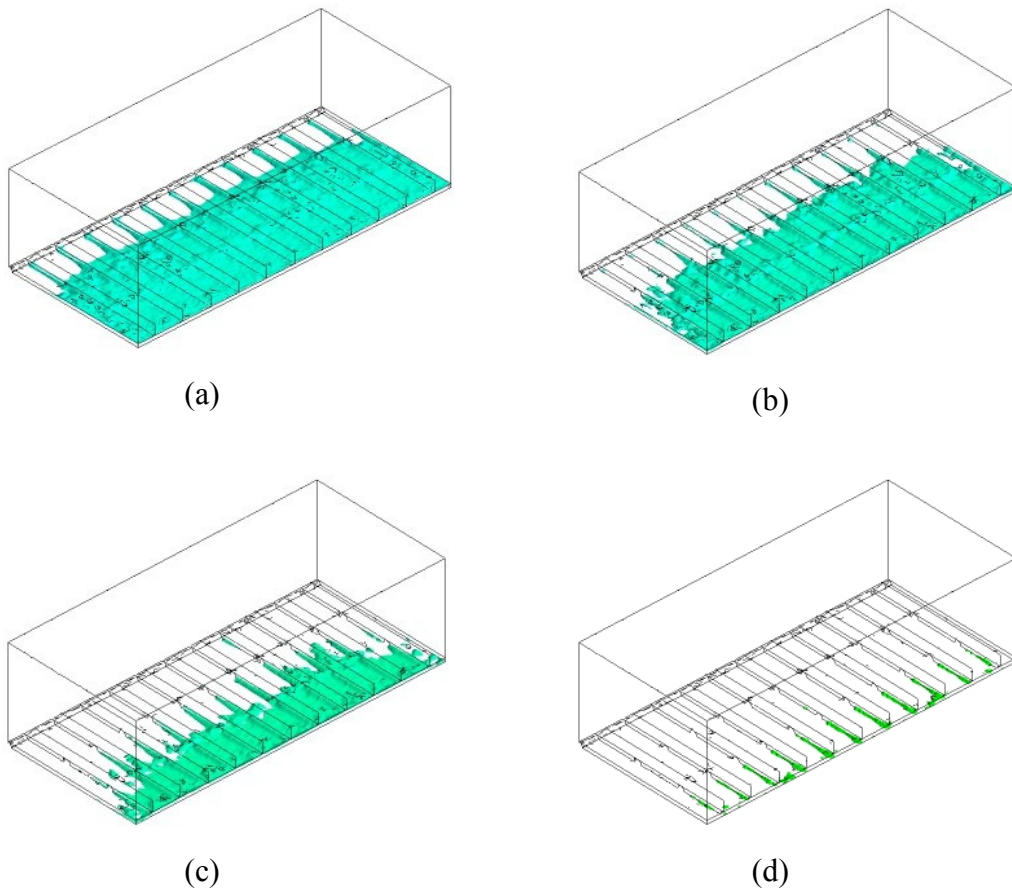
283

284　**Figure 6 Isosurface of sediments proportion above 2% at 600s with different**

285　**inlet velocity: (a) inlet velocity at 5 m/s; (b) inlet velocity at 10 m/s; (c) inlet**

286　**velocity at 15 m/s; (d) inlet velocity at 20 m/s**

287　These results visually show the remaining bottom sediments in the tank and it is found

288　that the sediments are suspended from the bottom left. With a higher inlet velocity,

289   more sediment on the bottom is suspended at the same moment. Besides, since the jet

290   holes are located in the midline of two bottom longitudinal plates, the sediments along

291   this midline are first suspended. Also, it is found the sediments on the bottom right of

292   the tank are latest suspended, thus the sediments proportion on the bottom right of the

293   tank can be monitored, which indicates the suspension conditions of the ballast tank.

294   Based on this observed results, the monitoring lines on the bottom right of the ballast

295   tank are introduced in this study to evaluate the suspension conditions, and the results

296   are discussed in the following section.

297   **5.2.   Average sediments proportion in initial sediments layer**

298   The proportion of sediments remaining in the ballast tank over time is investigated in

299   this study, and the results are obtained and shown in Figure 7 (a).

300   Generally, the simulation results show that the average sediments proportion in the

301   ballast tank decreases over time, and higher inlet velocity leads to a more rapid

302   decrease. To compare the simulation results with the experimental one, the time scale

303   is taken into account, and these results show good match. Further, the decreasing

304   speed is quantitatively analysed by introducing the 2% proportion line. Figure 7 (b)

305   shows the results within a more narrow range in x-axis. To reduce the sediments

306   proportion to fewer than 2%, less required time is needed with higher inlet velocity.

307   For the simulation results, the required time with inlet velocity at 5m/s, 10m/s, 15m/s,

308   20m/s are approximately 7200s (T_1), 2300s (T_2), 1250s (T_3) and 790s (T_4),

309   respectively. In comparison, the experimental required time, after being processed on

310   basis of the time scale, is obtained. The results show that the required time

311   (considering the time scale) are approximately 6670s ($\sqrt{l_r}$ $T_{1'}$), 2190s ($\sqrt{l_r}$ $T_{2'}$), 1180s

312   ($\sqrt{l_r}$ $T_{3'}$) and 680s ($\sqrt{l_r}$ $T_{4'}$), respectively.

313

(a)

314

(b)
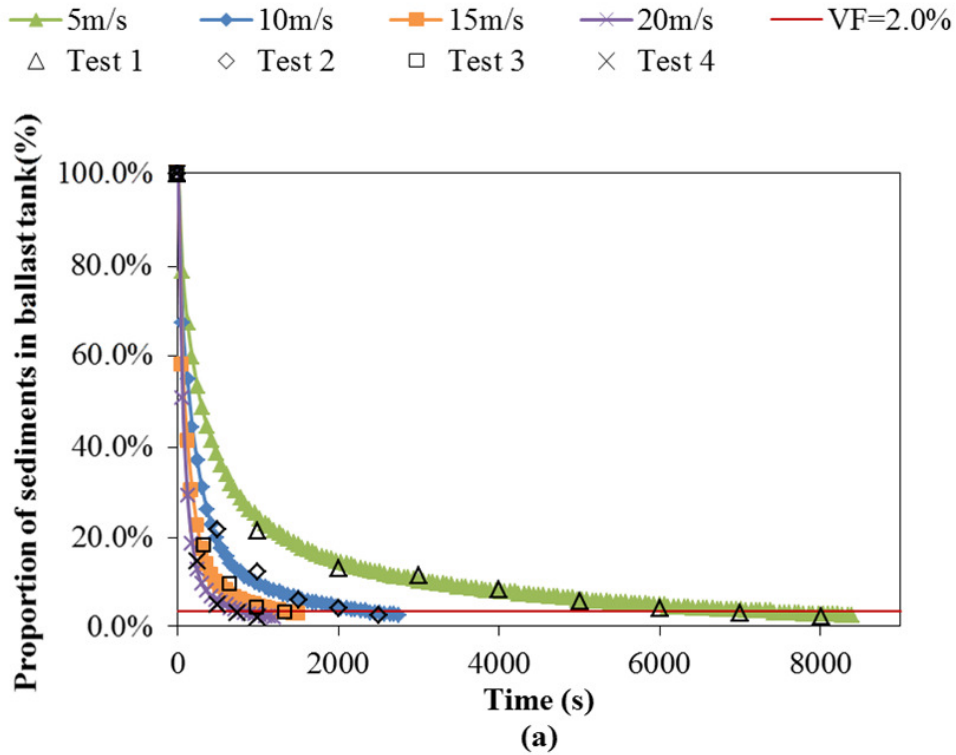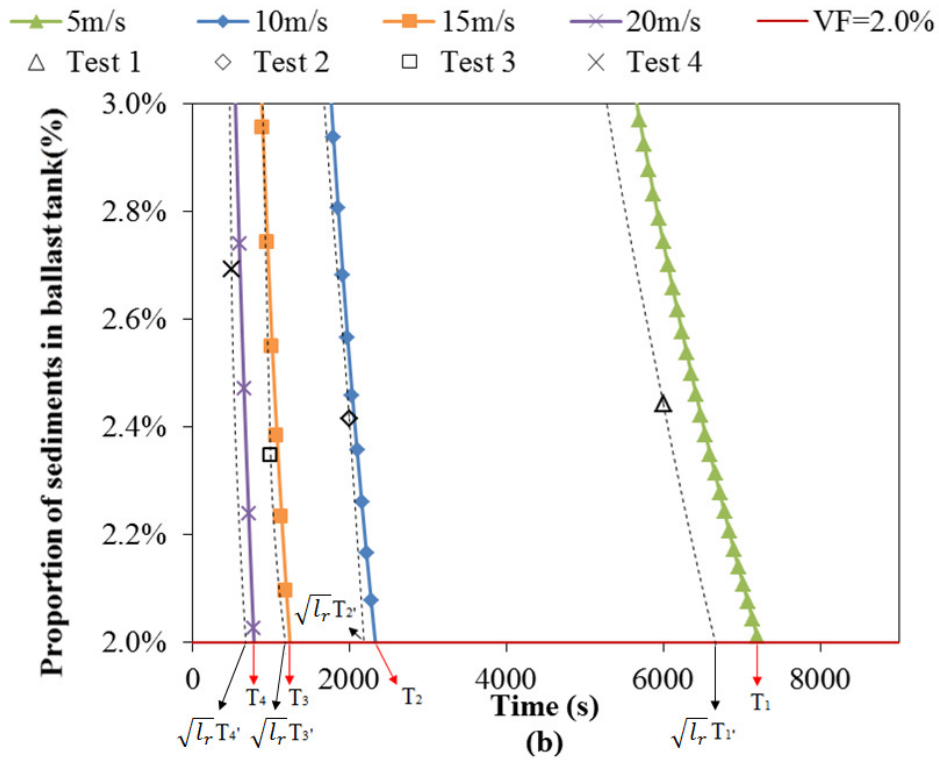
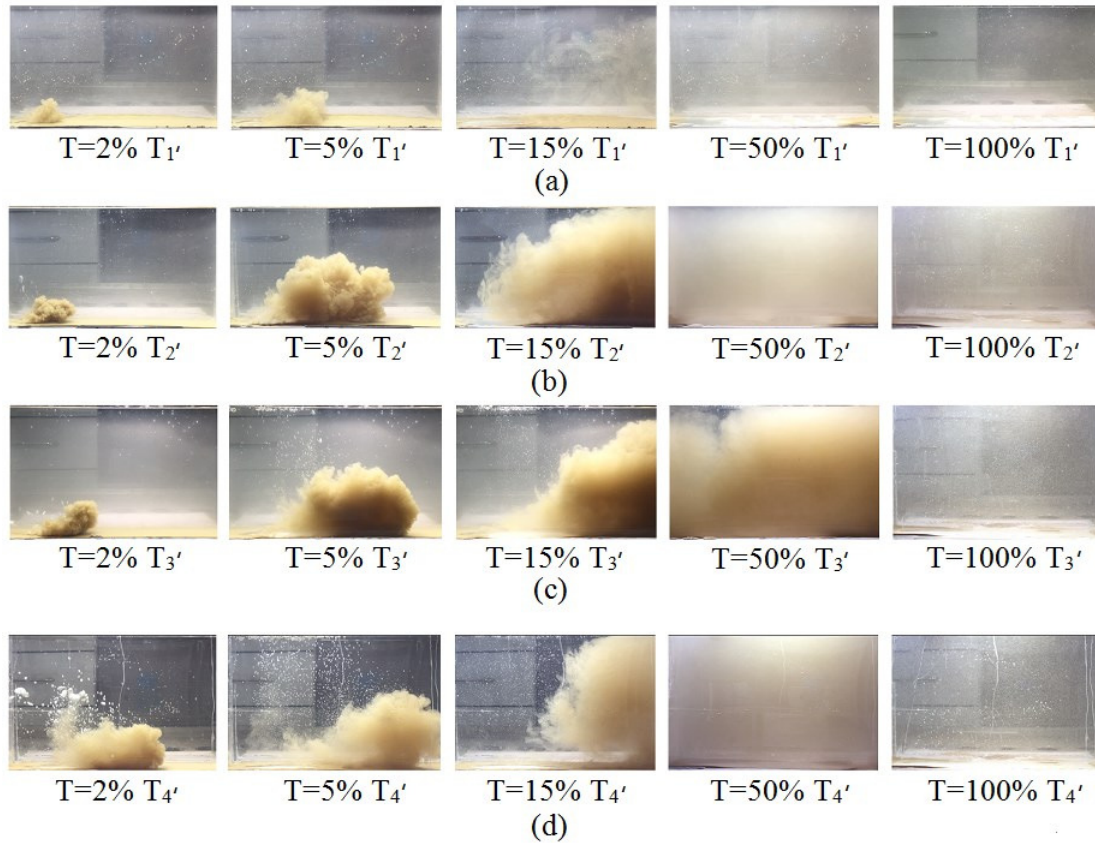315   **Figure 7 Average sediments proportion in initial sediments layer at different**

316   **inlet velocities**

5.3. Sediments distribution on the monitoring plane

Figure 8 shows the simulation results of sediments distribution on the monitoring plane as time varies. According to the simulation results in section 5.2, T_1, T_2, T_3, T_4 represent the required time of which the sediment are completely removed with 4 different inlet velocities. Further, a comparison study is made by the experiments, shown in Figure 9. With the assistance of these studies, the flushing process inside the ballast tank is observed. Generally, the sediments on the ballast tank bottom are first stirred up by the water injected from the jet holes, and then be sucked into the exit holes and get removed, remaining very small part of the sediments suspending in the ballast tank.

(a) T_1=7200s

(b) T_2=2300s

(c) T_3=1250s

(d) T_4=790s
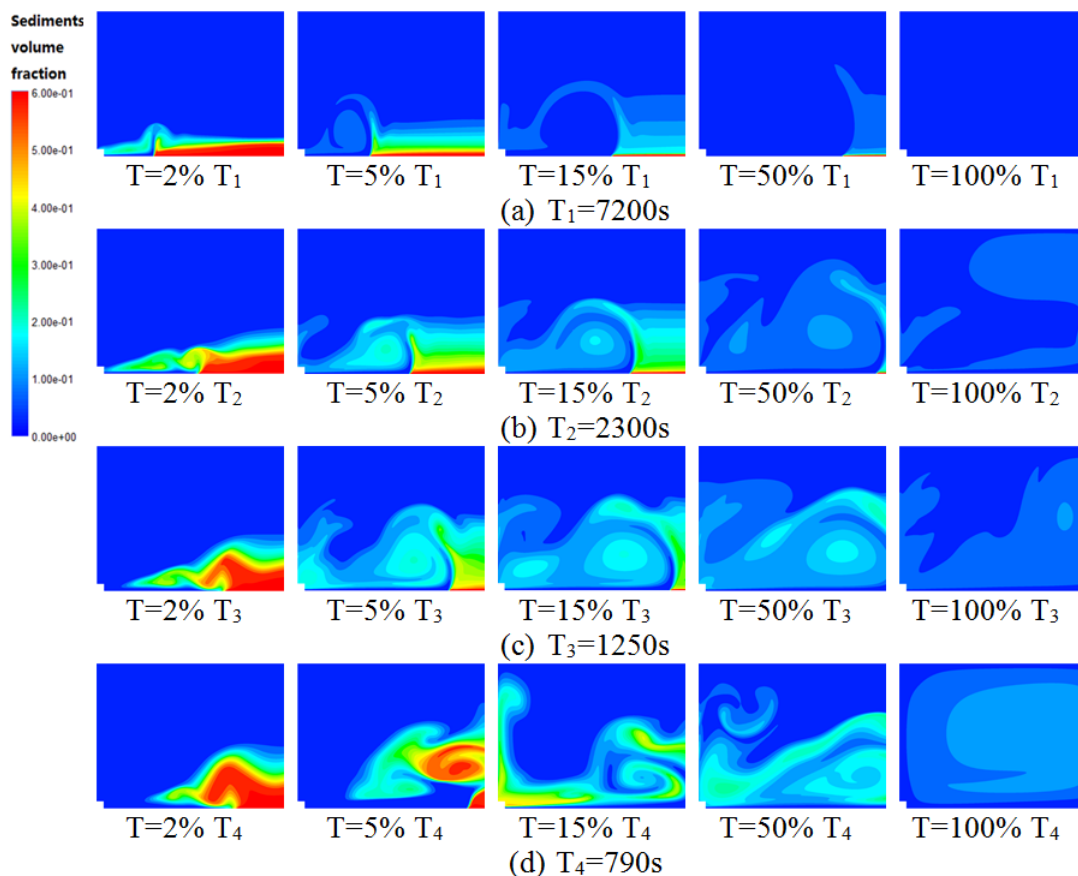
328   Figure 8 Simulation results of sediments distribution on the monitoring plane with

329   different inlet velocity: (a) inlet velocity at 5 m/s; (b) inlet velocity at 10 m/s; (c) inlet

330   velocity at 15 m/s; (d) inlet velocity at 20 m/s

| T=2% $T_{1'}$ | T=5% $T_{1'}$ | T=15% $T_{1'}$ | T=50% $T_{1'}$ | T=100% $T_{1'}$ |

(a)

| T=2% $T_{2'}$ | T=5% $T_{2'}$ | T=15% $T_{2'}$ | T=50% $T_{2'}$ | T=100% $T_{2'}$ |

(b)

| T=2% $T_{3'}$ | T=5% $T_{3'}$ | T=15% $T_{3'}$ | T=50% $T_{3'}$ | T=100% $T_{3'}$ |

(c)

| T=2% $T_{4'}$ | T=5% $T_{4'}$ | T=15% $T_{4'}$ | T=50% $T_{4'}$ | T=100% $T_{4'}$ |

(d)

331

332   Figure 9 Experimental results of sediments distribution with different inlet velocity: (a)

333   inlet velocity at 1.58 m/s; (b) inlet velocity at 3.16 m/s; (c) inlet velocity at 4.74 m/s;

334   (d) inlet velocity at 6.32 m/s

335   According to these results, the inlet velocity greatly affects the suspending of

336   sediments. With a lower inlet velocity, the sediments are gradually stirred up from

337   bottom left to right, while this process occurs drastically when the inlet velocity is at a

338   higher level. The removing process is observed from this figure. The bottom

339   sediments are suspended with the injected water, and then get discharged from the

340   exit holes. Also, lower inlet velocity means that much longer time is needed to fully

341 suspend the bottom sediments. As is shown in Figure 8 (a), it takes more than 7000s

342 to fully remove the sediments with the inlet velocity at 5m/s. Compared with this,

343 Figure 8 (d) shows that only approximately 900s is needed to get a similar result with

344 the inlet velocity at 20m/s. And similar phenomenon can be observed in the

345 experimental study.

346 **5.4. Average sediments volume fraction on the monitoring lines**

347 According to the initial conditions made in this simulation, the average sediments

348 volume fractions on each monitoring line are obtained, shown in Figure 10. Similarly,

349 the flow time is also selected as the variable parameter. Noting that when t=0s, the

350 corresponding sediments volume fraction on different monitoring lines are at different

351 values. As it was assigned in the initial conditions, for monitoring lines of z=0mm,

352 10mm and 20mm, the sediments volume fraction are all 60%; while for monitoring

353 lines of z=30mm and 40mm, this value are both at 0. As time varies, it is found that

354 the sediments volume fraction draw curves differently. On the monitoring lines of

355 z=0mm, 10mm and 20mm, where these lines are within the initial sediments layer, the

356 sediments volume fractions decrease rapidly from 60% to less than 20% over time,

357 and then they draw slightly decrease to 0. On the monitoring lines of z=30mm and

358 40mm, it is noted that the sediments volume fractions first climb up to 10-30% before

359 decrease gradually to 0. This is attributed to the following reason: as the sediments

360 near the jet holes are stirred up, they are entrained by the injected water and

361 accumulated on the right bottom of the ballast tank firstly, and then these sediments

362 are removed slightly over time. This phenomenon has also been detected in Figure 8

363 and Figure 9.

364   With different velocity at inflow-pipe inlet, the average sediments volume fractions of

365   ballast water at the same moment are also quite different. When t=1000s, the

366   sediments volume fractions on the tank bottom (z=0mm) are obtained. With inlet

367   velocity at 5m/s, 10m/s, 15m/s and 20m/s, this parameter decreases to approximately

368   22.3%, 8.6%, 2.5% and 1.3%, respectively. This indicates that higher inlet velocity

369   results in a better sediments suspension on the bottom. Besides of the tank bottom

370   monitoring line, other monitoring lines are all found decrease drastically as the inlet

371   velocity increases. Thus it is an effective method of removing the sediments by
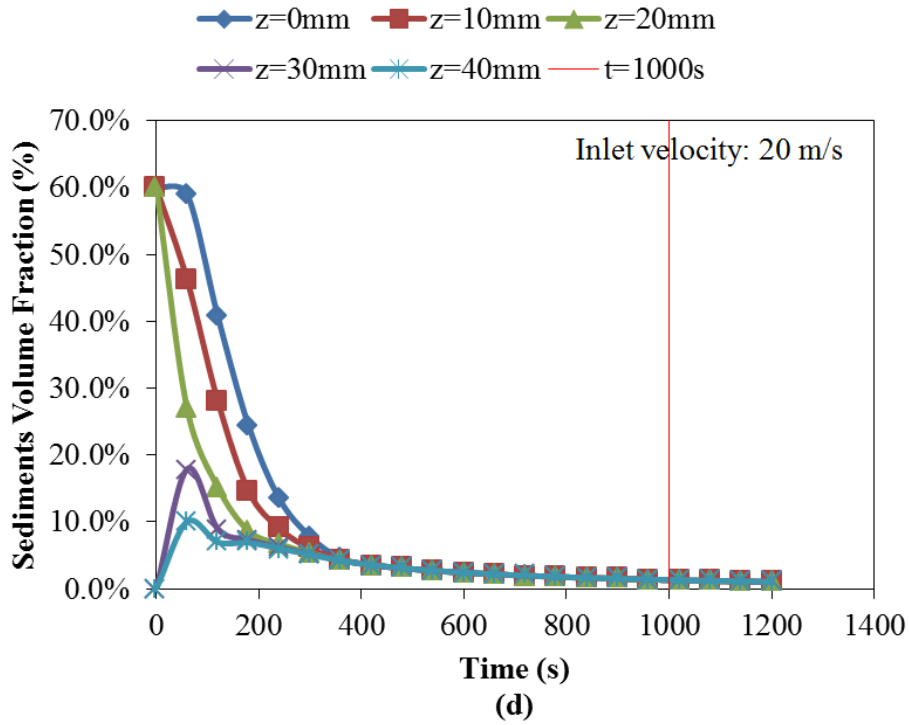
372   increasing the inlet velocity of inflow-pipe.

(a)

373

(b)

374

(c)

375
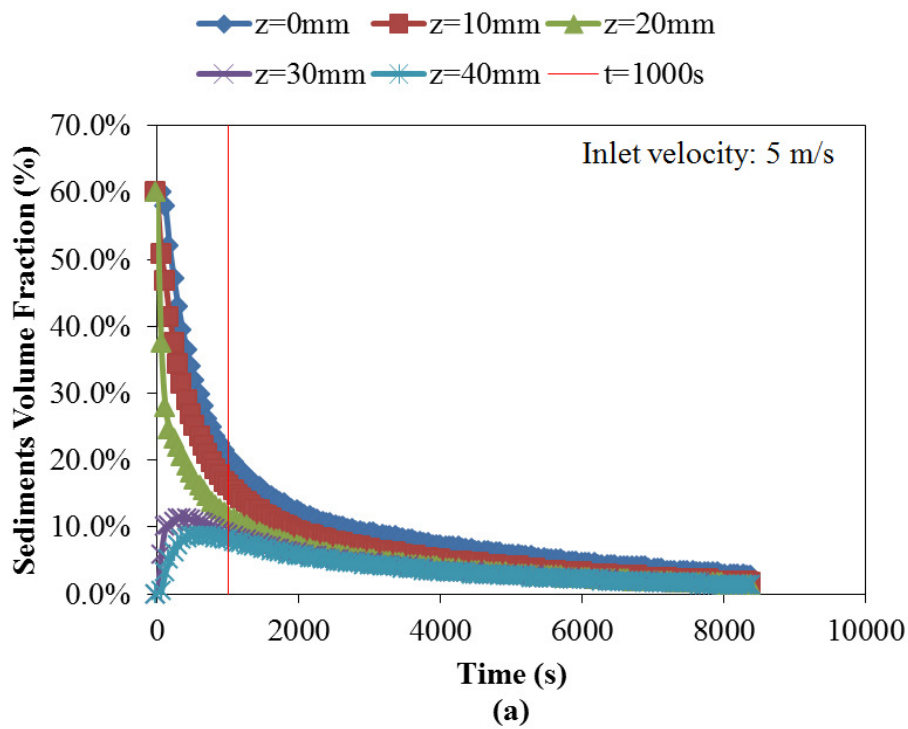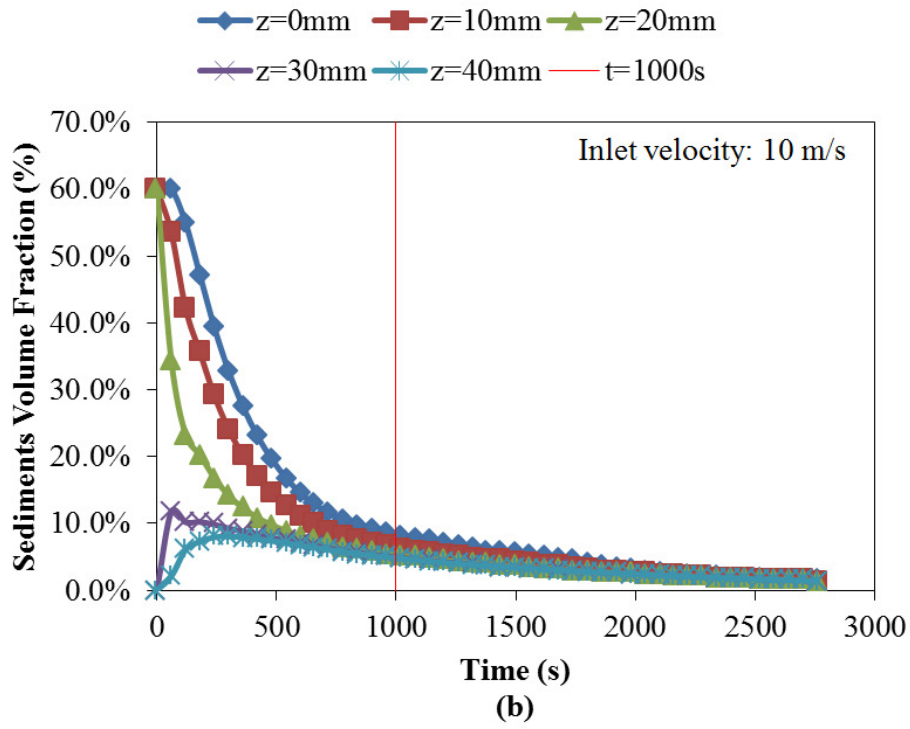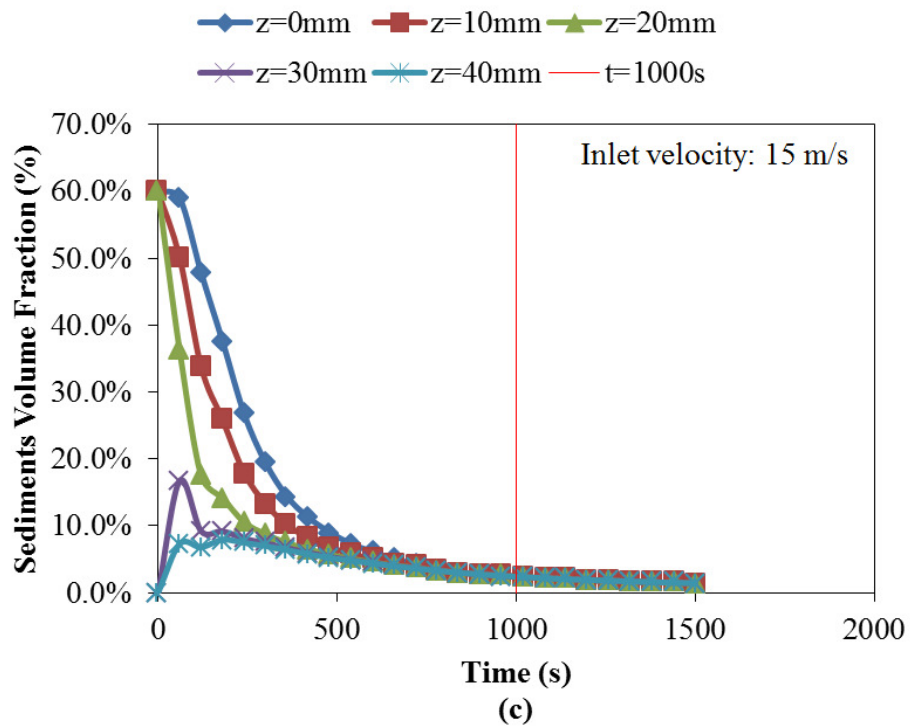
Figure 10 average sediments volume fraction on the monitoring lines

5.5. Energy consumption of the pump at different inlet velocities as the sediments proportion in initial sediments layer varies

Since the circulating pump is the only energy consumption component in this system, its energy consumption is the key parameter to evaluate the performance of this system. Generally, the energy consumption of the circulating pump is defined as:

$$W_P = (E_{bw} + W_{loss})\eta_P \tag{19}$$

$$E_{bw} = (P_0 - P_1)\dot{m}\Delta t / \rho_m \tag{20}$$

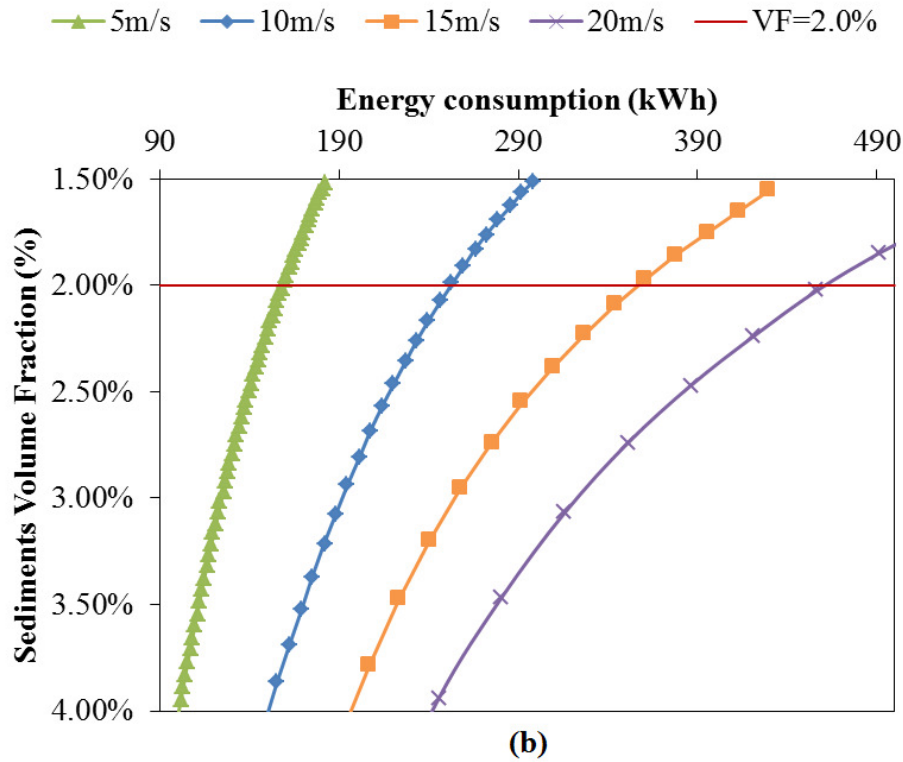$$P_0 + \frac{1}{2}\rho_m u_0 = P_1 + \frac{1}{2}\rho_m u_1 \tag{21}$$

$$W_{loss} = \Delta P_{loss}\dot{m}\Delta t / \rho_m \tag{22}$$

387   Where, E_{bw} is the total energy of the fluid in the ballast tank, P_0 and P_1 are the inlet

388   pressure of the inflow-pipe and the outlet pressure of the outflow-pipe, respectively,

389   W_{loss} is the energy losses of the pipe, ρ_m is the density of sediments-seawater mixture,

390 ΔP_{loss} is the pressure losses along the pipe.

(a)

391

392
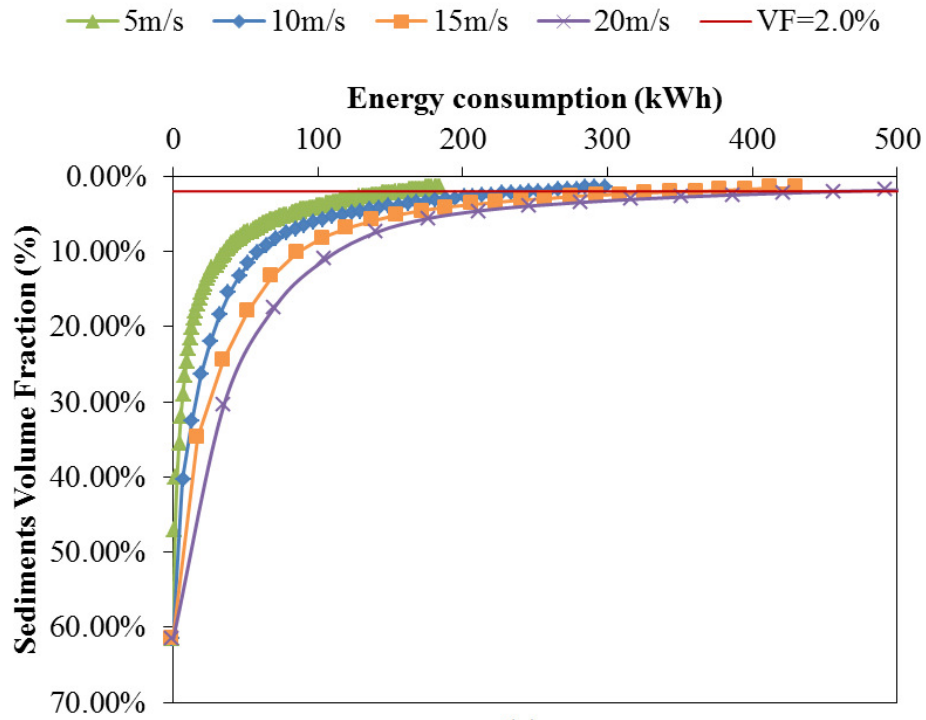
Figure 11 Energy consumption of circulating pump at different inlet velocities

According to Eq. (19-22), the energy consumption of the circulating pump is calculated and the results are shown in Figure 11. Generally, in order to get the same suspension effect, higher inlet velocity means higher energy consumption in circulating pump. The 2% sediments proportion line is also selected in this section as the critical line, which represents the fully suspension of the sediments. To reach this sediments proportion level, it is found that the energy consumption of 460kWh is required for inlet velocity at 20m/s. And this is followed by 356kWh, 252kWh and 156kWh for inlet velocity at 15m/s, 10m/s and 5m/s. These results are reasonable, for higher inlet velocity in inflow-pipe leads to higher kinetic energy of inject water and higher resistance losses in pipes and tank. Therefore, higher inlet velocity can increase the sediments removing speed; nevertheless, it can also result in higher energy consumption in circulating pump.
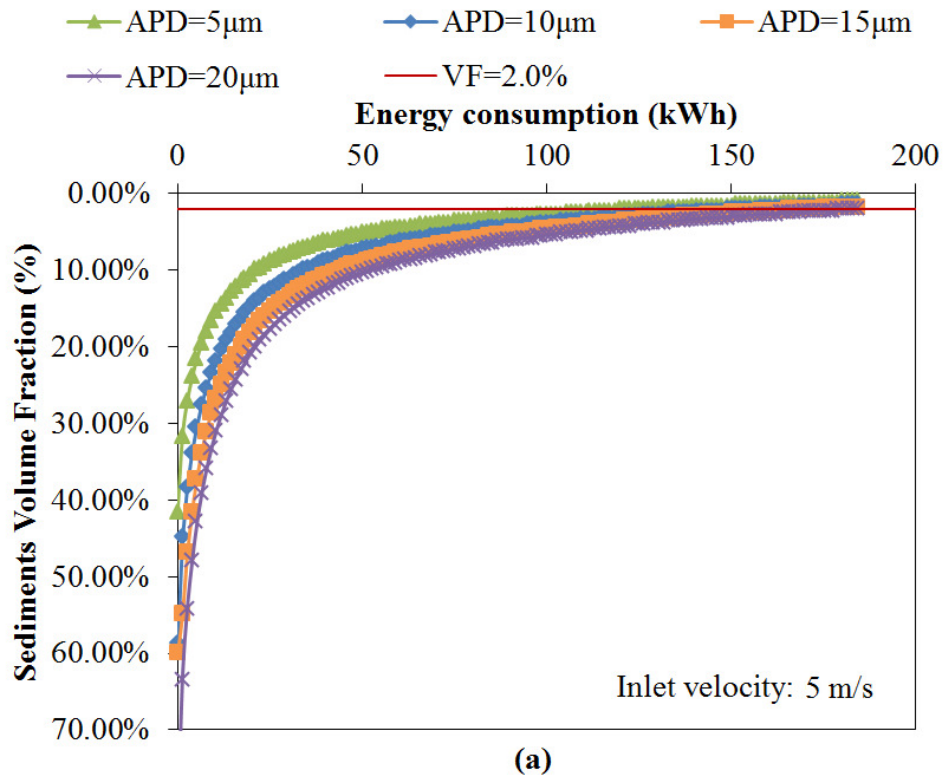
406
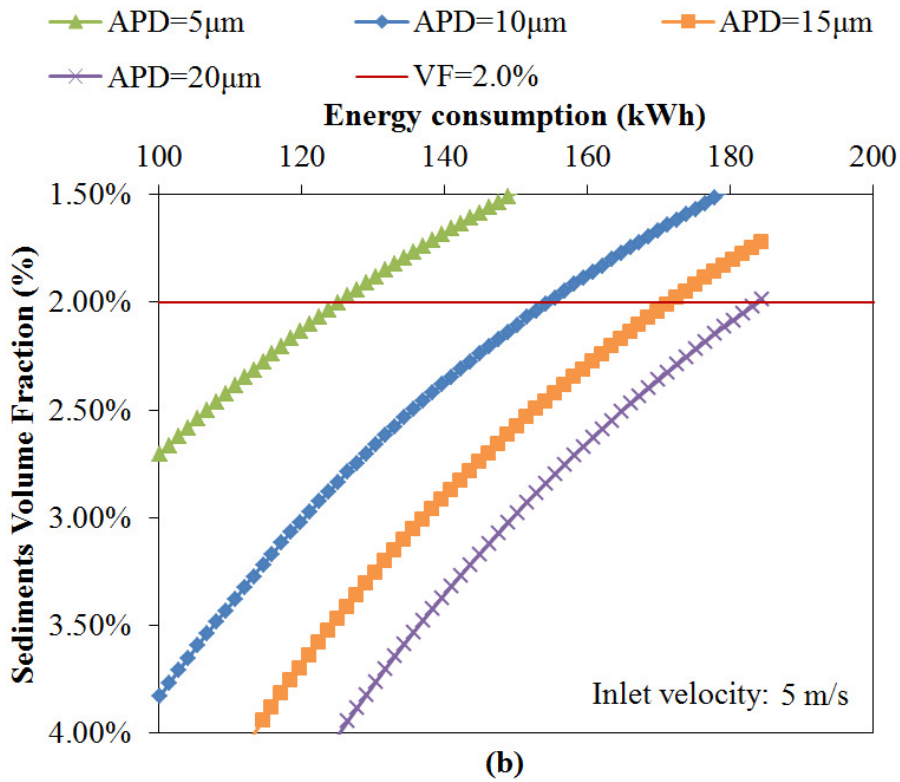
407

408 **Figure 12 Energy consumption of circulating pump as APD varies**

409 Further, the effect of particle size on the performance of ballast water flushing system

410 is investigated. The energy consumption of the circulating pump with 4 different

411 average particle diameters (APD, at 5, 10, 15, 20μm, respectively) is compared. The

412 inlet velocity of this system is chosen at 5m/s. The simulation results are shown in

413 Figure 12. The result indicates that more energy will be consumed with larger particle

414 size. To reach the 2% sediments proportion level, it is found the energy consumption

415 of 125kWh is required for APD at 5μm. This is follower by 154kWh, 171kWh,

416 184kWh for APD at 10, 15 and 20μm.

417

6. Conclusions

419 This study proposed a ballast water flushing system for ballast sediments removing

420 purpose. By circulating the ballast water, the deposited sediments on the bottom of the

421 ballast tank can be stirred up and separated in the hydrocyclone. With the assistance

422 of this system, no modification is needed for the tank structure. Also, the evacuating

423 of ballast water is needless during the sediments removing process. With the flushing

424 system, the unfiltered sediments along with the regrown organisms can be removed

425 when needed. This proposed flushing system could be considered as an alternative

426 technique for ballast water management. In this study, the simulation model for this

427 flushing system is made. Moreover, a 1:10 scaled experimental setup is established

428 based on the similarity principle. Both simulation and experimental investigation are

429 conducted to reveal the performance of this flushing system. Based on the analysis

430 made in this study, conclusions can be drawn as follows:

431 • The inlet velocity significantly affects the sediments removing efficiency. With

432   higher magnitude of inlet velocity, the required time for suspending sediments on

433   the bottom of the tank can be greatly decreased.

434   • The sediments on the bottom of the ballast tank first accumulate at the far end,

435   with the sediments volume fraction climbs up to 10-30%. Then these sediments

436   get removed over time and the sediments volume fraction decreases gradually to

437   0.

438   • Higher inlet velocity leads to a more rapid decrease of average sediments

439   proportion in the ballast tank over time. For the simulation results, the required

440   time for totally removing of sediments is approximately 7200s (with inlet velocity

441   at 5m/s), 2300s (10m/s), 1250s (15m/s) and 790s (20m/s), respectively. Similar

442   results are obtained from the experiments.

443   • To get the same suspension effect, higher inlet velocity means much higher

444   energy consumption in circulating pump. The energy consumption of 460kWh is

445   required (with inlet velocity at 20m/s), followed by 356kWh, 252kWh and

446   156kWh with inlet velocity at 15m/s, 10m/s and 5m/s, respectively. Besides,

447   more energy will be consumed with larger particle size.

448

453

454   **References**

455   [1] A. Djoghlaf, Convention on Biological Diversity (CBD), 2008.
456   [2] D.R. Scriven, C. DiBacco, A. Locke, T.W. Therriault, Ballast water management in Canada:
457   A historical perspective and implications for the future, Marine Policy, 59 (2015) 121-133.

458 [3] J.L. Molnar, R.L. Gamboa, C. Revenga, M.D. Spalding, Assessing the global threat of
459 invasive species to marine biodiversity, Frontiers in Ecology & the Environment, 6 (2008)
460 485-492.
461 [4] T.A. Shiganova, Invasion of the Black Sea by the ctenophore Mnemiopsis leidyi and recent
462 changes in pelagic community structure, Fisheries Oceanography, 7 (1998) 305–310.
463 [5] F. Pearce, How the Soviet seas were lost, New Scientist, (1995).
464 [6] M.A. Doblin, F.C. Dobbs, Setting a size-exclusion limit to remove toxic dinoflagellate cysts
465 from ships' ballast water, Marine Pollution Bulletin, 52 (2006) 259-263.
466 [7] M. Učur, International convention for the control and management of ships' ballast
467 water and sediments (imo, 2004), Naše more, Znanstveno-stručni časopis za more i
468 pomorstvo, 58 (2011) 124-131.
469 [8] J. Čulin, B. Mustać, Environmental risks associated with ballast water management
470 systems that create disinfection by-products (DBPs), Ocean & Coastal Management, 105
471 (2015) 100-105.
472 [9] B. Werschkun, S. Banerji, O.C. Basurko, M. David, F. Fuhr, S. Gollasch, T. Grummt, M.
473 Haarich, A.N. Jha, S. Kacan, Emerging risks from ballast water treatment: The run-up to the
474 International Ballast Water Management Convention, Chemosphere, 112 (2014) 256-266.
475 [10] A.N. Cohen, F.C. Dobbs, Failure of the public health testing program for ballast water
476 treatment systems, Marine Pollution Bulletin, 91 (2015) 29-34.
477 [11] N. Dobroski, C. Brown, R. Nedelcheva, C. Scianni, J. Thompson, 2015 Biennial Report on
478 the California Marine Invasive Species Program, (2015).
479 [12] F.L. Darby, Stemming the tide: Controlling introductions of nonindigenous species by
480 ships' ballast water : By National Research Council. National Academy Press, 1996. ISBN 0-
481 309-05537-7, US$39·95, Shanghai Coustruction Science & Technology, 35 (1997) 45-46.
482 [13] L. Maglić, D. Zec, V. Frančić, Ballast water sediment elemental analysis, Marine Pollution
483 Bulletin, 30 (2016) 68-72.
484 [14] A. Kremp, D.M. Anderson, Factors regulating germination of resting cysts of the spring
485 bloom dinoflagellate Scrippsiella hangoei from the northern Baltic Sea, Journal of Plankton
486 Research, 22 (2000) 1311-1327(1317).
487 [15] S. Itakura, M. Yamaguchi, Germination characteristics of naturally occurring cysts of
488 Alexandrium tamarense (Dinophyceae) in Hiroshima Bay, Inland Sea of Japan, Phycologia, 40
489 (2001) 263-267.
490 [16] R.I. Figueroa, I. Bravo, E. Garcés, I. Ramilo, NUCLEAR FEATURES AND EFFECT OF
491 NUTRIENTS ON GYMNODINIUM CATENATUM (DINOPHYCEAE) SEXUAL STAGES, Journal of
492 Phycology, 42 (2006) 67-77.
493 [17] J.P. Hamer, T.A. McCollin, I.A.N. Lucas, Dinoflagellate Cysts in Ballast Tank Sediments:
494 Between Tank Variability, Marine Pollution Bulletin, 40 (2000) 731-733.
495 [18] G. Prange, Ship Ballast Tank Sediment Reduction Methods, Naval Engineers Journal, 125
496 (2013) 127-134.
497 [19] I. Eames, M. Landeryou, A. Greig, J. Snellings, Continuous flushing of contaminants from
498 ballast water tanks, Marine Pollution Bulletin, 56 (2008) 250-260.
499 [20] I.A.o.C.S. (IACS), Guidelines for Coating Maintenance & Repairs for Ballast Tanks and
500 Combined Cargo/Ballast Tanks on Tankers, in: IACS Recommendation 87, 2006.
501 [21] M. Stipaničev, F. Turcu, L. Esnault, E.W. Schweitzer, R. Kilian, R. Basseguy, Corrosion
502 behavior of carbon steel in presence of sulfate-reducing bacteria in seawater environment,
503 Electrochimica Acta, 113 (2013) 390-406.
504 [22] Y. Lee, I. Sim, Y. Kim, J. Jung, J. Park, T. Jang, S. Kwon, Experimental study on sloshing for
505 large LNGC design, in: The Fifteenth International Offshore and Polar Engineering
506 Conference, International Society of Offshore and Polar Engineers, 2005.
507 [23] K. Pazouki, Inferential measurement and control of ballast water treatment system,
508 (2012).

509 [24] M. Shahrokhi, F. Rostami, M.M. Said, S. Syafalni, Numerical Modeling of the Effect of
510 the Baffle Location on the Flow Field, Sediment Concentration and Efficiency of the
511 Rectangular Primary Sedimentation Tanks, World Applied Sciences Journal, 15 (2011) 1296-
512 1309.
513 [25] B. Liu, J. Ma, L. Luo, Y. Bai, S. Wang, J. Zhang, Two-dimensional LDV measurement,
514 modeling, and optimal design of rectangular primary settling tanks, Journal of Environmental
515 Engineering, 136 (2009) 501-507.
516 [26] R. Tarpagkou, A. Pantokratoras, CFD methodology for sedimentation tanks: The effect
517 of secondary phase on fluid phase using DPM coupled calculations, Applied Mathematical
518 Modelling, 37 (2013) 3478-3494.
519 [27] A. Alvarado, S. Vedantam, P. Goethals, I. Nopens, A compartmental model to describe
520 hydraulics in a full-scale waste stabilization pond, Water research, 46 (2012) 521-530.
521 [28] A. Tamburini, A. Cipollina, G. Micale, A. Brucato, M. Ciofalo, CFD simulations of dense
522 solid–liquid suspensions in baffled stirred tanks: Prediction of solid particle distribution,
523 Chemical engineering journal, 223 (2013) 875-890.
524 [29] J. Hamer, Ballast Tank Sediments, in: E. Leppäkoski, S. Gollasch, S. Olenin (eds.) Invasive
525 Aquatic Species of Europe. Distribution, Impacts and Management, Springer Netherlands,
526 2002, pp. 232-234.
527 [30] S. Gollasch, The importance of ship hull fouling as a vector of species introductions into
528 the North Sea, (2002).
529 [31] A. Tamburini, A. Cipollina, G. Micale, A. Brucato, M. Ciofalo, CFD simulations of dense
530 solid–liquid suspensions in baffled stirred tanks: Prediction of the minimum impeller speed
531 for complete suspension, Chemical engineering journal, 193–194 (2012) 234-255.
532 [32] A. Tamburini, A. Cipollina, G. Micale, M. Ciofalo, A. Brucato, Dense solid–liquid off-
533 bottom suspension dynamics: Simulation and experiment, Chemical Engineering Research
534 and Design, 87 (2009) 587-597.
535 [33] A. Tamburini, A. Cipollina, G. Micale, A. Brucato, M. Ciofalo, CFD simulations of dense
536 solid–liquid suspensions in baffled stirred tanks: Prediction of suspension curves, Chemical
537 Engineering Journal, 178 (2011) 324–341.

538